
Concept-Centric Transformers: Concept Transformers with Object-Centric Concept Learning for Interpretability

Jinyung Hong

School of Computing and Augmented Intelligence
Arizona State University
Tempe, AZ 85281
jhong53@asu.edu

Theodore P. Pavlic

School of Computing and Augmented Intelligence
School of Sustainability
School of Complex Adaptive Systems
School of Life Sciences
Arizona State University
Tempe, AZ 85281
tpavlic@asu.edu

Abstract

Attention mechanisms have greatly improved the performance of deep-learning models on visual, NLP, and multimodal tasks while also providing tools to aid in the model’s interpretability. In particular, attention scores over input regions or concrete image features can be used to measure how much the attended elements contribute to the model inference. The recently proposed Concept Transformer (CT) generalizes the Transformer attention mechanism from such low-level input features to more abstract, intermediate-level latent concepts that better allow human analysts to more directly assess an explanation for the reasoning of the model about any particular output classification. However, the concept learning employed by CT implicitly assumes that across every image in a class, each image patch makes the same contribution to concepts that characterize membership in that class. Instead of using the CT’s image-patch-centric concepts, object-centric concepts could lead to better classification performance as well as better explainability. Thus, we propose *Concept-Centric Transformers (CCT)*, a new family of concept transformers that provides more robust explanations and performance by integrating a novel concept-extraction module based on object-centric learning. We test our proposed CCT against the CT and several other existing approaches on classification problems for MNIST (odd/even), CIFAR100 (super-classes), and CUB-200-2011 (bird species). Our experiments demonstrate that CCT not only achieves significantly better classification accuracy than all selected benchmark classifiers across all three of our test problems, but it generates more consistent concept-based explanations of classification output when compared to CT¹.

¹All source codes are available at https://github.com/jyhong0304/concept_centric_transformers.

1 Introduction

Although state-of-the-art machine-learning models have achieved remarkable performance across a wide range of applications, their intrinsic lack of transparency due to their many degrees of training freedom apparently limits their usage in safety-critical areas—such as medical diagnostics, healthcare, public infrastructure safety, and visual inspection for civil engineering—where trustworthy domain-specific knowledge is crucial for decision making. Toward explaining such black-box models, several recently developed methods provide *post hoc* explanations that identify relevant features that a trained model apparently uses to make predictions [45, 48, 51, 55]. However, these methods have been criticized for focusing only on low-level, concrete features that do not correspond to more abstract, high-level concepts that humans understand [1, 29, 30, 56]. To address these limitations, *intrinsically interpretable models* [50] have been proposed that make decisions based on human-understandable “concepts,” the foundation of domain expertise, instead of focusing on the raw features of the inputs [1, 3, 7, 8, 16, 20, 28, 29, 32, 38, 67, 71]. These methods enable high-level concepts to be used that can mimic human thinking processes structured in familiar concepts and provide insight into model reasoning that is easier for humans to understand. The gap between *post hoc* explainability and intrinsically interpretable models also is discussed in the NLP community in respect to interpreting *attention mechanisms* [2]. In particular, the debate over what degree of interpretability can be ascribed to attention weights over input tokens still needs to be settled to help meet the need for interpretability of attention mechanisms [1, 5, 27, 52, 63].

The *Concept Transformer (CT)* [49] is an intrinsically interpretable model with attention mechanism that has been proposed to improve an arbitrary deep-learning classifier with domain knowledge based on cross-attention weights between input features and high-level interpretable concepts. The CT was devised to provide explanations that guarantee: i) *faithfulness by design* [22, 35] by applying a linear relationship between the learnable concept vectors and their contribution to the classification log probabilities, and ii) *plausibility by construction* [5, 22] by governing the attention heads of the cross-attention mechanism [59] to reinforce inputs–concepts–outputs relations from domain knowledge. Learning concepts from the input in the CT can be leveraged generally to represent specific concepts, such as *global* or *spatial* concepts. The CT uses an image-patch-level concept extraction that can be beneficial when trying to incorporate a small number of global concepts given the task or extract spatial concepts from the input. However, it may be limited in cases aiming to extract scalable global concepts from an image because each image patch in the input, even though it belongs to the same class, may have different importance in providing the information of that concept. Also, focusing on image patches to extract spatial information sometimes hinders the model’s classification performance because it acts as “noise” that causes the model to focus only on small regions instead of global ones. Thus, extracting global concepts from images requires a new model capable of learning how each image patch contributes to the corresponding concept.

We propose the *Concept-Centric Transformer (CCT)*, a new family of CT that incorporates with a novel global concept extraction method based on object-centric learning. The CCT consists of two architectural components: i) **Concept-Slot-Attention module** that interfaces with image patches from the patch-based architectures and that produces a set of task-dependent embedding for concepts, and ii) **Cross-Attention module** that generates classification outputs using cross-attention between input features and a set of concept embedding from the concept-slot-attention module. The improved concept-learning method in CCT has no appreciable increase in overhead relative to CT yet extracts better global concepts based on each batch of inputs, which evidently contributes to better classification performance. We validate our approach on three image benchmark datasets—MNIST Odd/Even [3], CIFAR100 Super-class [14], and CUB-200-2011 [61]—combining it with various deep-learning backbones, such as Vision Transformer (ViT) [12] and hybrid Compact Convolutional Transformer models [23]. We investigate how to apply CCT to provide domain-relevant explanations in faithful and plausible ways behind specific output decisions and how the global concepts extracted by the CCT contribute to better classification performance by analyzing the results. Finally, by comparing attention scores, we show that CCT is a quantitative and qualitative improvement over CT.

2 Related Work

Significant advances have recently been made in devising explainable and interpretable models to measure the importance of individual features for predictive output. The *post hoc* analysis is one

general approach to analyzing a trained model by matching explanations to classification outputs [1, 45, 48]. For example, activation maximization [47, 58, 68] and saliency visualization [51, 55, 57] are well-known methods for CNNs. However, *post hoc* methods do not provide an explanation of how a model arrives at a specific classification outcome. To address this issue, attention-based interpretable approaches have been introduced to identify the most relevant parts of the input that the network focuses on when making a decision [15, 17, 18, 25, 73, 74, 75, 76]. However, these models require improvement as they focus on low-level individual features when providing explanations. When interpreted afterward, these features can be noisy, misleading, and non-intuitive for humans [29].

Designing methods that explain predictions with high-level, human-understandable concepts [3, 7, 8, 16, 20, 28, 29, 32, 38, 49, 66, 67, 71] is one of the recent advancements in the field of interpretability. These intrinsically interpretable methods focus on identifying common activation patterns in the nodes of last layer of the neural network corresponding to human-understandable categories or constraining the network to learn such concepts. The recently proposed CT [49] learns high-level concepts defined with a set of related dimensions. Those concepts, which can be part-specific or global, typically are able to boost the performance of the learning task while offering explainability at no additional cost to the network. Furthermore, obtained explanations are plausible and faithful because concepts participate in the model computation. However, the approach relies on extracting image-patch-based concepts, ignoring that each image patch can be an unreliable predictor of high-level concepts.

There have been many approaches to developing neural networks operating on unordered *sets* of features [37, 60, 70]. The concept extraction module in our work is closely related to the object-centric approaches that use a set of latent variables (“slots”) to model permutation-invariant aspects of the input [21, 43], such as objects in images. Referring to them as slot-centric methods, this class of models forms the fundamental for many modern scene-understanding approaches that apply to various vision tasks—such as video dynamics [13, 31, 64], unsupervised object detection and discovery [21, 43, 54], visual reasoning tasks [46], and reinforcement learning [6]. Our work explores an interpretable, concept-centric approach based on slot-centric models, allowing for better interpretability and performance.

3 Concept-Centric Transformers

In this section, we introduce the architecture of Concept-Centric Transformers (CCTs), consisting of: i) *Concept-Slot-Attention module* (§3.1) that extracts the latent concept embedding representation from input, and ii) *Cross-Attention module* (§3.2) among the input and the extracted concept embedding from the Concept-Slot-Attention module to produce faithful and plausible concept-based explanations. The overall architecture of our proposed module is summarized in Fig. 1. Rather than focusing on image features with the same spatial position, as in CT [49], our CCT can learn concepts decoupled from image position; further details about this CT–CCT comparison are discussed in Appendix B.

3.1 Concept-Slot Attention Module

We propose *Concept-Slot Attention (CSA) module* as a novel concept learning mechanism based on slot attention [43]. The CSA module encodes a set of L input feature vectors \mathbf{E} into concept representations $\mathbf{S}^{\text{concept}}$, which we refer to as *concept slots*. The CSA module is a general-purpose mechanism that, in principle, can be used for any input modality as long as it is provided as a set of vectors. Therefore, it can be seen as a drop-in module plugged into any arbitrary neural architecture.

Concept Binding Specific to Each Input Batch. With the user-defined number of concepts C , the concept slots $\mathbf{S}^{\text{concept}} \in \mathbb{R}^{C \times d}$ first perform competitive attention [43] on the input features $\mathbf{E} \in \mathbb{R}^{L \times D}$. For this, we apply linear projection q^{CSA} on the concept slots to obtain the queries and projections k^{CSA} and v^{CSA} on the inputs to obtain the keys and the values, all having the same size d^2 . Then, we perform a dot-product between the queries and keys to get the attention matrix $\mathbf{A}^{\text{CSA}} \in \mathbb{R}^{C \times L}$. In \mathbf{A}^{CSA} , each entry $\mathbf{A}_{c,l}^{\text{CSA}}$ is the attention weight of concept slot c for attending over the input vector l . We normalize \mathbf{A}^{CSA} by applying softmax across concept slots, i.e., along the axis C . This implements a form of competition among slots for attending to each input l .

²For simplicity, the embedding size d is shared equally within our proposed method.

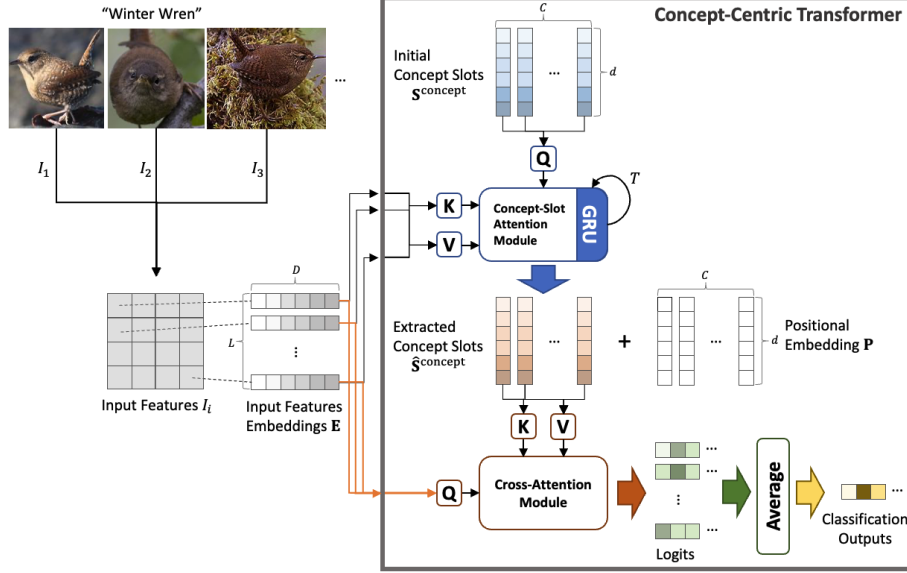


Figure 1: Overall architecture of Concept-Centric Transformers (CCTs). The CCT is a drop-in replacement for the classifier head of an arbitrary deep-learning classifier and consists of two modules: (1) Concept-Slot-Attention module and (2) Cross-Attention module. The figure shows a CCT as the classifier head of a patch-based architecture like a ViT or a patch-level CNN.

We then seek to group and aggregate the attended inputs and obtain the attention readout for each concept slot. Intuitively, this can be seen as how much the attended inputs contribute to semantically representing each concept. For this, we normalize the attention matrix $\mathbf{A}^{\text{CSA}} \in \mathbb{R}^{C \times L}$ along the axis L and multiply it with the input values $v^{\text{CSA}}(\mathbf{E}) \in \mathbb{R}^{L \times d}$. This produces the attention readout in the form of a matrix $\mathbf{U} \in \mathbb{R}^{C \times d}$ where each row $u_c \in \mathbb{R}^d$ is the readout corresponding to concept slot c .

$$\mathbf{A}^{\text{CSA}} = \text{softmax}_C \left(\frac{q^{\text{CSA}}(\mathbf{S}^{\text{concept}}) \cdot k^{\text{CSA}}(\mathbf{E})^\top}{\sqrt{d}} \right), \quad \mathbf{A}_{c,l}^{\text{CSA}} = \frac{\mathbf{A}_{c,l}^{\text{CSA}}}{\sum_{l=1}^L \mathbf{A}_{c,l}^{\text{CSA}}}, \quad \mathbf{U} = \mathbf{A}^{\text{CSA}} \cdot v^{\text{CSA}}(\mathbf{E})$$

We use the readout information obtained from concept binding and update each concept slot. The aggregated updates \mathbf{U} are finally used to update the concept slots via a learned recurrent function, for which we use a Gated Recurrent Unit (GRU) [9] with d hidden units so that $\mathbf{S}^{\text{concept}} = \text{GRU}(\mathbf{S}^{\text{concept}}, \mathbf{U})$. The processes above form one refinement iteration. Here, we set the number of iterations T to 1, but the refinement could be repeated several times depending on the tasks. The concept slots obtained from the last iteration are considered final. The overall module is described in Algorithm 1 in pseudo-code in Appendix B.

Positional Embedding for Concept Slots. Because the resulting set of concept slots is order-less [43], it is difficult for the later module to: (i) recognize which high-level concept each concept slot is representing and (ii) identify which concept slot each high-level concept belongs to. Thus, we add a positional encoding \mathbf{p}_c to each concept slot to avoid these challenges; in particular, $\hat{\mathbf{s}}_c = \mathbf{s}_c + \mathbf{p}_c$. After this, the concept embedding representation $\hat{\mathbf{S}}^{\text{concept}} \in \mathbb{R}^{C \times d}$ with positional embedding \mathbf{P} is passed as the final concept representation to the next module.

3.2 Cross-Attention (CA) Module For Concept-Slots-based Interpretability

Similar to CT [49], we define the *Cross-Attention (CA) module*, a successor module combined with the previous CSA module to be used as classifier head in a deep-learning architecture that generates classification outputs using cross-attention between input features and their concept embeddings extracted from the CSA module. Similar to the previous CSA module, a set of L input feature vectors $\mathbf{E} \in \mathbb{R}^{L \times D}$ are re-used with a linear projection q^{CA} to attain the queries, and projections k^{CA} and v^{CA} are applied to the extracted concept slots with position embedding $\hat{\mathbf{S}}$ from the CSA module. The resulting keys and values are used in a cross-attention mechanism with the queries, and the

cross-attention then outputs an attention weight $\mathbf{A}^{\text{CA}} \in \mathbb{R}^{L \times C}$

$$\mathbf{A}^{\text{CA}} = \text{softmax}_L \left(\frac{q^{\text{CA}}(\mathbf{E}) \cdot k^{\text{CA}}(\hat{\mathbf{S}}^{\text{concept}})^\top}{\sqrt{d}} \right)$$

between each patch-concept slot pair. The final output of the CA module comes from taking the product obtained by multiplying the attention map \mathbf{A}^{CA} , the values $v^{\text{CA}}(\hat{\mathbf{S}}^{\text{concept}}) \in \mathbb{R}^{C \times d}$, and an output matrix $\mathbf{O} \in \mathbb{R}^{d \times n_c}$ that projects onto the (unnormalized) n_c logits over the output classes and then averaging over input features³; that is,

$$\text{logit}_i = \frac{1}{L} \sum_{l=1}^L \mathbf{A}_l^{\text{CA}} \cdot v^{\text{CA}}(\hat{\mathbf{S}}^{\text{concept}}) \cdot \mathbf{O}_{:,i} \quad \text{for } i = 1, \dots, n_c.$$

So, given an input \mathbf{x} to the network, the conditional probability of output class $i \in \{1, \dots, n_c\}$ is:

$$\Pr(i|\mathbf{x}) = \text{softmax}_i \left(\sum_{c=1}^C \beta_c \gamma_c(\mathbf{x}) \right) \quad \text{with } \beta_c \text{ components } (\beta_c)_i := (v^{\text{CA}}(\hat{\mathbf{S}}^{\text{concept}}) \cdot \mathbf{O})_{c,i} \quad (1)$$

where $\gamma_c(\mathbf{x})$ are non-negative relevance scores that depend on \mathbf{x} through the averaged attention weights; that is, $\gamma_c(\mathbf{x}) = \frac{1}{L} \sum_{l=1}^L \mathbf{A}_{l,c}^{\text{CA}}$. Essentially, the CA module output is a multinomial logistic regression model over positive variables $\gamma_c(\mathbf{x})$ that measures the contribution of each concept slot.

Faithful Concept-slot-based Explanations by Design. *Faithfulness* is the degree to which explanation reflects the decision and aims to ensure that the explanations are indeed explaining model operation [22, 35]. Similar to CT, the result of the CA module follows the linear relation between the value vectors and the classification logits and comes from the design choices of computing outputs from the value matrix $v^{\text{CA}}(\hat{\mathbf{S}}^{\text{concept}})$ through the linear projection $v^{\text{CA}}(\hat{\mathbf{S}}^{\text{concept}}) \cdot \mathbf{O}$ and aggregating patch contributions by averaging. Therefore, our CA module is also guaranteed to be faithful by design by satisfying Proposition 1 in [49], including the technical definitions of [1].

3.3 Training and Plausibility by Construction

As shown in the CSA–CA integration above, our CCT is formed as a differentiable transformer-based module embedded in a deep-learning architecture trained end-to-end with backpropagation. *Plausibility* refers to how convincing the interpretation is to humans [5, 22]. To provide plausible human-understandable explanations, our module displays attention weights on concept tokens that users can customize, enabling the attention weights to be based on domain expertise about the specific problem by explicitly guiding the attention heads to focus on concepts in the input that are important for correctly classifying the input. Similar to [11], given a desired distribution of attention \mathbf{H} provided by domain knowledge, the attention weights from the CA module of the CCT \mathbf{A}^4 are used as a regularization term by adding an *explanation cost* to the objective function that is proportional to $\mathcal{L}_{\text{expl}} = \|\mathbf{A} - \mathbf{H}\|_F^2$, where $\|\cdot\|$ is the Frobenius norm. Thus, the final loss used to train the architecture then becomes $\mathcal{L} = \mathcal{L}_{\text{cls}} + \lambda \mathcal{L}_{\text{expl}}$, where \mathcal{L}_{cls} denotes the original classification loss, $\mathcal{L}_{\text{expl}}$ the additional explanation loss, and the constant $\lambda \geq 0$ controls the relative contribution of the explanation loss to the total loss. That is, setting $\lambda = 0$ minimizes classification loss only, and we set $\lambda > 0$ to incentivize explainability.

4 Experiments

We evaluate our CCT on three datasets: MNIST Odd/Even [1], CIFAR100 Super-class [14], and CUB-200-2011 [61]. The different datasets showcase various use cases and visual backbones combined with the CCT to show the adaptability and versatility of the CCT module. All experimental results are performed with three different random seeds and 95% confidence intervals unless we provide particular references with the results. Further experimental details can be seen in Appendix C.

³For simplicity, we have described a single-head attention model here, but in practice, a multi-head version [59] is available and is also used in our experiments.

⁴Precisely, the relevance score vector $\gamma(\mathbf{x}) \in \mathbb{R}^C$.

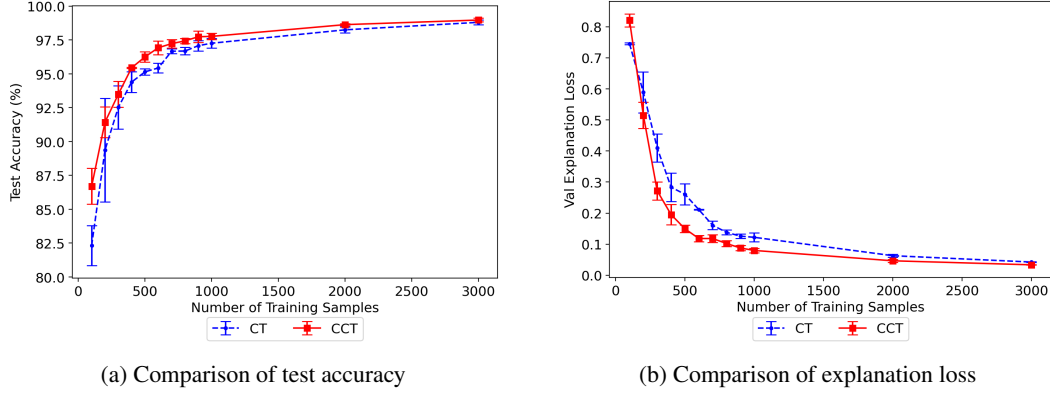


Figure 2: Sample-efficiency gain of using explanations at training on the MNIST Odd/Even dataset.

4.1 Evaluation on MNIST Odd/Even

The MNIST Odd/Even task is a binary classification task based on the MNIST Odd/Even dataset where 28x28-pixel images of hand-written digits of MNIST [36] ranging from 0 to 9 should be classified as either ‘even’ or ‘odd.’ In this case, we exploit each digit’s identity as an *explanation* for the class prediction. For instance, a ‘2’ should be classified as ‘even,’ and a plausible explanation to support this prediction is that *it is ‘even’ because it is a ‘2’* (left example in Fig. 3). We follow the experiments in [49] and consider a relatively simple case where the correspondence between concepts and output classes is many-to-one and deterministic and global concepts are used. We simply assume that the concepts refer to the whole input, essentially equivalent to having only one patch. For the task, we combine our CCT with a small Compact Convolutional Transformer architecture [23].

For this task, using the full training samples, CT and CCT both achieve test accuracy close to 99% even when trained with very few epochs (10), and so we compare these models when fewer samples are used. Figure 2 shows the test accuracy and explanation loss during validation relative to the number of samples used at training, which varies from 100 to 3000, for both CT and our new CCT. CCT outperforms CT in terms of both test accuracy and validation explanation loss.

Figure 3 shows several test samples predicted by both methods. The left example is correctly classified as ‘even’ because both achieved the highest attention score of ‘2’. Conversely, from two other more problematic cases, we highlight that our CCT can achieve more valuable concept attention scores than CT. The middle case (a ‘4’) is incorrectly classified as an ‘odd.’ As shown in the concept attention scores in both CT and our CCT, the incorrect prediction can be traced back to the fact that both models strongly associated the sample with the ‘9’ concept and thereby predicted the sample to be ‘odd’. However, the attention score of ‘4’, the correct explanation, in our CCT is higher than the one in CT, showing the better efficacy of CCT for concept learning. This observation is even starker in the example on the right of Fig. 3. Further results and details can be found in Appendix C.4.

4.2 Evaluation on CIFAR100 Super-class

The CIFAR100 Super-class dataset is a variant of the CIFAR100 [34] image dataset. It consists of 100 classes of images that are further grouped into 20 super-classes. For instance, the five classes

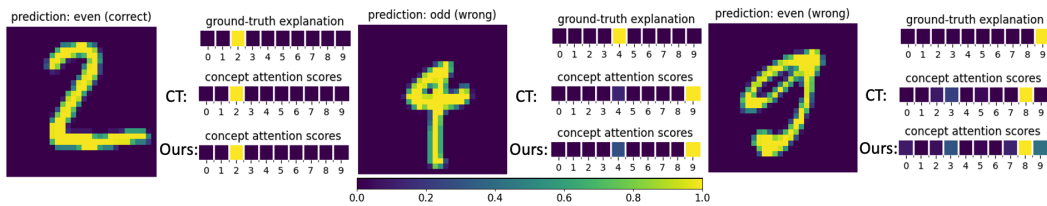


Figure 3: Examples of predictions on MNIST Odd/Even and comparison of attention scores between CT and CCT. (Left) Correct predictions. (Middle and Right) Incorrect predictions.

Model	Class Accuracy (%)	Super-class Accuracy (%)
Vanilla ResNet [†]	NA	83.2 \pm 0.2
Vanilla ViT-Tiny	NA	86.2 \pm 0.3
Hierarchical Model [†]	71.2 \pm 0.2	84.7 \pm 0.1
DL2 [†] [14]	75.3 \pm 0.1	84.3 \pm 0.1
MultiplexNet [†] [24]	74.4 \pm 0.2	85.4 \pm 0.3
CT [49]	73.3 \pm 2.9	92.1\pm0.2
CCT (ours)	80.3\pm0.4	92.6\pm0.1

Table 1: Accuracy on class and super-class label prediction. [†] indicates results from [24].

baby, boy, girl, man, and woman belong to the super-class *people*. Since the introduction of *deep-learning models with logical constraints* [14], this dataset has been used as one of the benchmark datasets to assess the effectiveness of embedding the constraints into neural networks (in-depth surveys can be found in [10, 19]). We show that the concepts in our CCT (and CT) can be naively seen as “constraints” (the difference between CCT and other methods with logical constraints is described in Appendix C.5) and that enforcing additive contributions from user-defined concepts to the classification log probabilities can similarly act to enforce satisfying the constraints. We exploit each image class as an explanation for the multiclass prediction task with 20 super-classes and use a Vision Transformer-Tiny (ViT-Tiny) as a backbone for this dataset. As inputs to the CCT handling the global concepts, we use the embedding of the CLS token.

Following [24], we compare the performance of our CCT to three baseline groups. The first group is vanilla backbone models, including a ‘Wide ResNet 28-10’ [69] and ‘ViT-Tiny.’ The Wide ResNet was used as a backbone for the second baseline group. The first baseline group is trained to predict the super-class labels only, and so they cannot predict class labels. Based on the ResNet as a backbone, the second baseline group is neural-network models with logical constraints, including: i) ‘Hierarchical Model’ in [24], trained to predict the super-class label and, thereafter, the fine class label, conditioned on the value for the super-class label, ii) ‘DL2’ [14], and iii) ‘MultiplexNet’ [24]. Both DL2 and MultiplexNet are deep-learning frameworks that exploit logical constraints. Finally, the third group of models is transformer-based explainable models, including CT and our CCT with ViT-Tiny as the backbone. To evaluate class accuracy for CT and CCT, we compared the ground-truth concept explanation to the predicted concept with the top-1 highest attention score by the trained models.

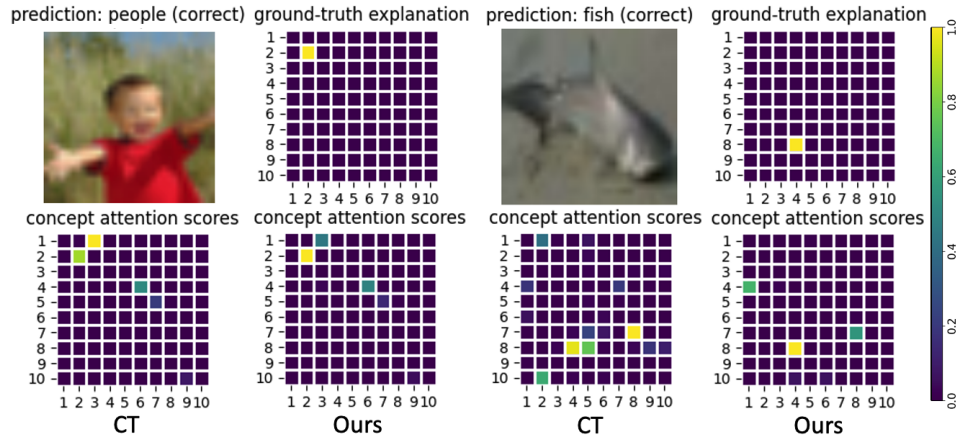


Figure 4: Comparison of class predictions for CT and our CCT (“Ours”) in examples where both make correct CIFAR100 super-class predictions. The 100 classes are indexed from 1 (top left in 10x10 grid) to 100 (bottom right in 10x10 grid). **(Left)** Ground-truth class label is *boy* (12), but CT mispredicted it as *baby* (3), whereas our CCT’s prediction is correct. **(Right)** Ground-truth label is *shark* (84), but CT incorrectly selects *ray* (78) while our CCT again makes a correct class prediction.

Table 1 presents the experimental results for the task. First, Vanilla ViT-Tiny outperforms Wide ResNet despite having far fewer parameters (5.5M for ViT-Tiny and 36.5M for ResNet). Both CT and CCT use a ViT-Tiny backbone and so are also parameter efficient (5.7M for CT and 6M for CCT) compared to the ResNet backbone. However, for super-class test accuracy, CT and our CCT achieve the best performances, 92.1% and 92.6%, respectively, significantly improving the performance of their ViT-Tiny backbone alone.

Our CCT also achieves the best performance in class test accuracy (80.3%), which is starkly better than CT (73.3%), which itself is worse in class accuracy than logic-constraint-based approaches. This shows that our module better contributes to forming global concepts than CT. Fig. 4 introduces two examples, depicting that our CCT’s concept learning method is better quantitatively and qualitatively than CT and that CT’s poor performance of class accuracy might be the case making *hallucinations* to greedily achieve super-class accuracy without forming sound concepts. The super-classes of both examples are correctly classified by CT and our CCT, but the explanatory decision-making processes perform entirely differently in the two models. Although the ground-truth class of the left image in Fig. 4 is *boy*, the best-matching class concept with the highest attention score by CT was *baby*, which is the incorrect class but also belongs to the correct super-class *people*. From the right example, we observe a similar behavior of CT. In contrast, our CCT’s predicted concepts for both examples correctly match their ground-truth classes with sparser concept attention scores than CT. Further details and results are described in Appendix C.5.

4.3 Evaluation on CUB-200-2011

The CUB-200-2011 [61] dataset includes 11788 images of birds classified into 200 species. Each image has annotations with a given number of discrete concepts, e.g., the shape of the beak, or the color of the body, describing the visual attributes of the bird in the image that could aid in the identification of the species of a particular bird. The dataset uses 312 concepts, but their distribution varies across images, and so we leverage a pre-processing method from [49] for the dataset that retains only concepts present in at least 45% of the images in each class and subsequently present in at least 9 classes, leading to retaining 108 concepts.

We consider a real-world case where the relation between concepts and outputs is many-to-many and non-deterministic, and a mixture of *global* and *spatially localized* concepts exists. We instantiate two processes to handle both concepts: i) using both CSA and CA modules in the CCT for global concepts and ii) using only the CA module with the learnable vectors for spatial concepts. We then average the logits provided by both to preserve interpretability. We use a Vision Transformer (ViT-Large) for this dataset as a backbone. We use the embeddings of the tokenized image patches, while as input to the CCT in charge of the concepts, we use the embedding of the CLS token.

Table 2 compares our CCT against other approaches, grouped based their use of *Multi-stage* (i.e., complex training) or *End-to-end* (i.e., training with backpropagation) training. Our CCT achieves 90% classification accuracy, showing a distinct performance improvement over other approaches, including CT. Thus, the global concepts extracted by CCT indeed boost the overall performance of the classification task. Our model’s test accuracy surpasses the non-interpretable baseline model (B-CNN) and others (e.g., MA-CNN); additionally, some methods require extremely more complex

Method	Test Accuracy (%)			
Multi-stage	Part R-CNN: 76.4	PS-CNN: 76.2	PN-CNN: 85.4	SPDA-CNN: 85.1
	PA-CNN: 82.8	MG-CNN: 83.0	2-level attn.: 77.9	FCAN: 82.0
	Neural const.: 81.0	ProtoPNet: 84.8		
End-to-end	B-CNN: 85.1	CAM: 70.5	DeepLAC: 80.3	ST-CNN: 84.1
	MA-CNN: 86.5	RA-CNN: 85.3	CEM: 77.1	ProtoPFormer: 84.9
	CT: 86.4 \pm 0.2	CCT (ours): 90.0 \pm 0.3		

Table 2: Performance comparison on CUB-200-2011. For B-CNN [41], Part R-CNN [73], PS-CNN [25], PN-CNN [4], SPDA-CNN [72], PA-CNN [33], MG-CNN [62], 2-level attn. [65], FCAN [42], Neural const. [53], ProtoPNet [7], CAM [75], DeepLAC [40], ST-CNN [26], MA-CNN [74], and RA-CNN [15], performance from [49]. For ProtoPFormer [66] and CEM [71], best performance directly from their works. For CT [49] and CCT, results from our evaluation.

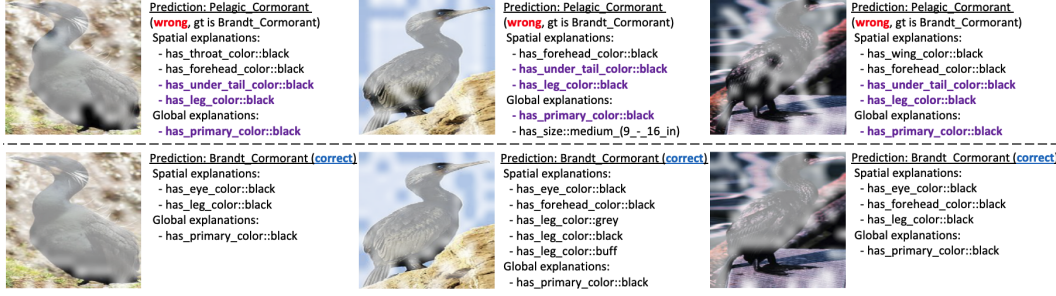


Figure 5: Prediction comparison between CT and our CCT. **(Top)** All CT’s predictions are incorrect. The highlighted explanations in purple are key attributes typically present when correctly classifying Pelagic_Cormorant, the incorrect label. **(Bottom)** Our CCT’s predictions are correct.



Figure 6: Prediction comparison between CT and our CCT. **(Top)** CT’s predictions are incorrect. **(Bottom)** All predictions are correct by our CCT.

training than our CCT. For the type of explanations provided, CAM and CEM emphasize the entire object as the reason behind a classification decision at the coarsest level. In contrast, most models present part-level attention at a finer level but in a different way than how attention is generated. For example, Part R-CNN, SPDA-CNN, PS-CNN, and PN-CNN employ further part-localization models previously trained with part annotations. While RA-CNN uses an extra neural network to determine where to focus attention, MA-CNN uses convolutional feature maps to direct attention to various image parts. ProtoPNet uses previously learned prototypes to direct its attention to a specific region of an input image, similar to a prototypical example that has been learned. But, because it is based on part-level concepts, object-level concepts cannot be easily incorporated, and *post hoc* analysis is required to find learned prototypes for other models. ProtoPFormer, a family of ProtoPNet, was proposed recently to incorporate both global and local concepts with a simpler training process, but it still requires multiple steps of *post hoc* analysis.

Figures 5 and 6 demonstrate the contrasts between CT and our CCT, where the image-patch-centric CT lacks learning of global concepts. We emphasize concepts with the highest attention scores in all images. Figure 5 shows a case where the CT’s predictions were completely incorrect by converging to the single wrong label. Although the ground-truth class of the images was Brandt_Cormorant, all CT’s predictions were Pelagic_Cormorant. Furthermore, the attributes CT used to make the incorrect classification included a subset of attributes (purple-colored attributes in Fig. 5) typically associated with correct predictions of the incorrect Pelagic_Cormorant label. Thus, the image-patch-centric CT hallucinates key aspects associated with incorrect labels whereas our CCT shows more robust global explanations of correct classifications. Also, Fig. 6 depicts a case where the CT’s predictions were utterly different from each other despite all images having the same class. The predicted classes from the CT in Fig. 6 were Prothonotary_Warbler, Pine_Warbler, and Magnolia_Warbler, respectively. The only difference between the first two predictions that the CT made is whether the spatial concept `has_under_tail_color::black` exists, indicating the CT’s performance sensitivity. In addition, the third prediction from the CT contains new spatial concepts unrelated to the first two examples, which shows analytical uncertainty as to why the CT made such a decision. In contrast, the predictions made by our CCT were all correct, with consistent global explanations. This indicates that although incorporating spatial concepts provide

additional information, determining robust global concepts is more important for the classification task. Additional results and details are described in Appendix C.6.

5 Conclusions

We proposed Concept-Centric Transformers, an elaboration of the Concept Transformer with a novel global concept extraction module based on the slot-centric method to ensure better interpretability of attention scores and better classification performance. Using three benchmark image datasets, we showed that the explanations obtained are plausible, faithful, and have good performance. A natural future research direction is to extend the concept extraction module to acquire composable “pieces” of knowledge [54] and then learn the underlying composition rules or mechanisms relating the acquired pieces to each other. Those rules can be formed in logical rules, such as first-order logic [3]. It is also promising to investigate other applications, such as model debugging and medical-image diagnosis.

References

- [1] D. Alvarez Melis and T. Jaakkola. Towards robust interpretability with self-explaining neural networks. *Advances in Neural Information Processing Systems*, 31, 2018.
- [2] D. Bahdanau, K. Cho, and Y. Bengio. Neural machine translation by jointly learning to align and translate. *arXiv preprint arXiv:1409.0473*, 2014.
- [3] P. Barbiero, G. Ciravegna, F. Giannini, P. Lió, M. Gori, and S. Melacci. Entropy-based logic explanations of neural networks. In *Proceedings of the AAAI Conference on Artificial Intelligence*, volume 36, pages 6046–6054, 2022.
- [4] S. Branson, G. Van Horn, S. Belongie, and P. Perona. Bird species categorization using pose normalized deep convolutional nets. *arXiv preprint arXiv:1406.2952*, 2014.
- [5] D. V. Carvalho, E. M. Pereira, and J. S. Cardoso. Machine learning interpretability: A survey on methods and metrics. *Electronics*, 8(8):832, 2019.
- [6] M. Chang, A. L. Dayan, F. Meier, T. L. Griffiths, S. Levine, and A. Zhang. Neural constraint satisfaction: Hierarchical abstraction for combinatorial generalization in object rearrangement. *arXiv preprint arXiv:2303.11373*, 2023.
- [7] C. Chen, O. Li, D. Tao, A. Barnett, C. Rudin, and J. K. Su. This looks like that: deep learning for interpretable image recognition. *Advances in Neural Information Processing Systems*, 32, 2019.
- [8] Z. Chen, Y. Bei, and C. Rudin. Concept whitening for interpretable image recognition. *Nature Machine Intelligence*, 2(12):772–782, 2020.
- [9] K. Cho, B. van Merriënboer, C. Gulcehre, D. Bahdanau, F. Bougares, H. Schwenk, and Y. Bengio. Learning phrase representations using RNN encoder–decoder for statistical machine translation. In *Proceedings of the 2014 Conference on Empirical Methods in Natural Language Processing (EMNLP)*, pages 1724–1734, 2014.
- [10] T. Dash, S. Chitlangia, A. Ahuja, and A. Srinivasan. A review of some techniques for inclusion of domain-knowledge into deep neural networks. *Scientific Reports*, 12(1):1040, 2022.
- [11] A. Deshpande and K. Narasimhan. Guiding attention for self-supervised learning with transformers. *arXiv preprint arXiv:2010.02399*, 2020.
- [12] A. Dosovitskiy, L. Beyer, A. Kolesnikov, D. Weissenborn, X. Zhai, T. Unterthiner, M. Dehghani, M. Minderer, G. Heigold, S. Gelly, et al. An image is worth 16x16 words: Transformers for image recognition at scale. *arXiv preprint arXiv:2010.11929*, 2020.
- [13] G. Elsayed, A. Mahendran, S. van Steenkiste, K. Greff, M. C. Mozer, and T. Kipf. Savi++: Towards end-to-end object-centric learning from real-world videos. *Advances in Neural Information Processing Systems*, 35:28940–28954, 2022.

- [14] M. Fischer, M. Balunovic, D. Drachsler-Cohen, T. Gehr, C. Zhang, and M. Vechev. DL2: training and querying neural networks with logic. In *International Conference on Machine Learning*, pages 1931–1941. PMLR, 2019.
- [15] J. Fu, H. Zheng, and T. Mei. Look closer to see better: Recurrent attention convolutional neural network for fine-grained image recognition. In *Proceedings of the IEEE Conference on Computer Vision and Pattern Recognition*, pages 4438–4446, 2017.
- [16] A. Ghorbani, J. Wexler, J. Y. Zou, and B. Kim. Towards automatic concept-based explanations. *Advances in Neural Information Processing Systems*, 32, 2019.
- [17] R. Girshick. Fast R-CNN. In *Proceedings of the IEEE International Conference on Computer Vision*, pages 1440–1448, 2015.
- [18] R. Girshick, J. Donahue, T. Darrell, and J. Malik. Rich feature hierarchies for accurate object detection and semantic segmentation. In *Proceedings of the IEEE Conference on Computer Vision and Pattern Recognition*, pages 580–587, 2014.
- [19] E. Giunchiglia, M. C. Stoian, and T. Lukasiewicz. Deep learning with logical constraints. *arXiv preprint arXiv:2205.00523*, 2022.
- [20] Y. Goyal, A. Feder, U. Shalit, and B. Kim. Explaining classifiers with causal concept effect (CaCE). *arXiv preprint arXiv:1907.07165*, 2019.
- [21] K. Greff, R. L. Kaufman, R. Kabra, N. Watters, C. Burgess, D. Zoran, L. Matthey, M. Botvinick, and A. Lerchner. Multi-object representation learning with iterative variational inference. In *International Conference on Machine Learning*, pages 2424–2433. PMLR, 2019.
- [22] R. Guidotti, A. Monreale, S. Ruggieri, F. Turini, F. Giannotti, and D. Pedreschi. A survey of methods for explaining black box models. *ACM Computing Surveys (CSUR)*, 51(5):1–42, 2018.
- [23] A. Hassani, S. Walton, N. Shah, A. Abuduweili, J. Li, and H. Shi. Escaping the big data paradigm with compact transformers. *arXiv preprint arXiv:2104.05704*, 2021.
- [24] N. Hoernle, R. M. Karampatsis, V. Belle, and K. Gal. Multiplexnet: Towards fully satisfied logical constraints in neural networks. In *Proceedings of the AAAI Conference on Artificial Intelligence*, volume 36, pages 5700–5709, 2022.
- [25] S. Huang, Z. Xu, D. Tao, and Y. Zhang. Part-stacked CNN for fine-grained visual categorization. In *Proceedings of the IEEE Conference on Computer Vision and Pattern Recognition*, pages 1173–1182, 2016.
- [26] M. Jaderberg, K. Simonyan, A. Zisserman, et al. Spatial transformer networks. *Advances in Neural Information Processing Systems*, 28, 2015.
- [27] S. Jain and B. C. Wallace. Attention is not explanation. *arXiv preprint arXiv:1902.10186*, 2019.
- [28] D. Kazhdan, B. Dimanov, M. Jamnik, P. Liò, and A. Weller. Now you see me (CME): concept-based model extraction. *arXiv preprint arXiv:2010.13233*, 2020.
- [29] B. Kim, M. Wattenberg, J. Gilmer, C. Cai, J. Wexler, F. Viegas, et al. Interpretability beyond feature attribution: Quantitative testing with concept activation vectors (TCAV). In *International Conference on Machine Learning*, pages 2668–2677. PMLR, 2018.
- [30] P.-J. Kindermans, S. Hooker, J. Adebayo, M. Alber, K. T. Schütt, S. Dähne, D. Erhan, and B. Kim. The (un) reliability of saliency methods. *Explainable AI: Interpreting, explaining and visualizing deep learning*, pages 267–280, 2019.
- [31] T. Kipf, G. F. Elsayed, A. Mahendran, A. Stone, S. Sabour, G. Heigold, R. Jonschkowski, A. Dosovitskiy, and K. Greff. Conditional object-centric learning from video. *arXiv preprint arXiv:2111.12594*, 2021.
- [32] P. W. Koh, T. Nguyen, Y. S. Tang, S. Mussmann, E. Pierson, B. Kim, and P. Liang. Concept bottleneck models. In *International Conference on Machine Learning*, pages 5338–5348. PMLR, 2020.

- [33] J. Krause, H. Jin, J. Yang, and L. Fei-Fei. Fine-grained recognition without part annotations. In *Proceedings of the IEEE Conference on Computer Vision and Pattern Recognition*, pages 5546–5555, 2015.
- [34] A. Krizhevsky. Learning multiple layers of features from tiny images. Master’s thesis, University of Toronto, Toronto, Canada, 2009.
- [35] H. Lakkaraju, E. Kamar, R. Caruana, and J. Leskovec. Faithful and customizable explanations of black box models. In *Proceedings of the 2019 AAAI/ACM Conference on AI, Ethics, and Society*, pages 131–138, 2019.
- [36] Y. LeCun. The MNIST database of handwritten digits. <http://yann.lecun.com/exdb/mnist/>, 1998.
- [37] J. Lee, Y. Lee, J. Kim, A. Kosiorek, S. Choi, and Y. W. Teh. Set transformer: A framework for permutation-invariant neural networks. In *International Conference on Machine Learning*, pages 3744–3753. PMLR, 2019.
- [38] O. Li, H. Liu, C. Chen, and C. Rudin. Deep learning for case-based reasoning through prototypes: A neural network that explains its predictions. In *Proceedings of the AAAI Conference on Artificial Intelligence*, volume 32, 2018.
- [39] Z. Li, Z. Liu, Y. Yao, J. Xu, T. Chen, X. Ma, L. Jian, et al. Learning with logical constraints but without shortcut satisfaction. In *The Eleventh International Conference on Learning Representations*, 2023.
- [40] D. Lin, X. Shen, C. Lu, and J. Jia. Deep lac: Deep localization, alignment and classification for fine-grained recognition. In *Proceedings of the IEEE Conference on Computer Vision and Pattern Recognition*, pages 1666–1674, 2015.
- [41] T.-Y. Lin, A. RoyChowdhury, and S. Maji. Bilinear CNN models for fine-grained visual recognition. In *Proceedings of the IEEE International Conference on Computer Vision*, pages 1449–1457, 2015.
- [42] X. Liu, T. Xia, J. Wang, Y. Yang, F. Zhou, and Y. Lin. Fully convolutional attention networks for fine-grained recognition. *arXiv preprint arXiv:1603.06765*, 2016.
- [43] F. Locatello, D. Weissenborn, T. Unterthiner, A. Mahendran, G. Heigold, J. Uszkoreit, A. Dosovitskiy, and T. Kipf. Object-centric learning with slot attention. *Advances in Neural Information Processing Systems*, 33:11525–11538, 2020.
- [44] I. Loshchilov and F. Hutter. Decoupled weight decay regularization. *arXiv preprint arXiv:1711.05101*, 2017.
- [45] S. M. Lundberg and S.-I. Lee. A unified approach to interpreting model predictions. *Advances in Neural Information Processing Systems*, 30, 2017.
- [46] S. S. Mondal, T. W. Webb, and J. Cohen. Learning to reason over visual objects. In *Proceedings of the Eleventh International Conference on Learning Representations*, 2023.
- [47] A. Nguyen, A. Dosovitskiy, J. Yosinski, T. Brox, and J. Clune. Synthesizing the preferred inputs for neurons in neural networks via deep generator networks. *Advances in Neural Information Processing Systems*, 29, 2016.
- [48] M. T. Ribeiro, S. Singh, and C. Guestrin. "why should i trust you?" explaining the predictions of any classifier. In *Proceedings of the 22nd ACM SIGKDD international conference on knowledge discovery and data mining*, pages 1135–1144, 2016.
- [49] M. Rigotti, C. Mikovic, I. Giurciu, T. Gschwind, and P. Scotton. Attention-based interpretability with concept transformers. In *International Conference on Learning Representations*, 2021.
- [50] C. Rudin. Stop explaining black box machine learning models for high stakes decisions and use interpretable models instead. *Nature Machine Intelligence*, 1(5):206–215, 2019.

- [51] R. R. Selvaraju, M. Cogswell, A. Das, R. Vedantam, D. Parikh, and D. Batra. Grad-cam: Visual explanations from deep networks via gradient-based localization. In *Proceedings of the IEEE International Conference on Computer Vision*, pages 618–626, 2017.
- [52] S. Serrano and N. A. Smith. Is attention interpretable? *arXiv preprint arXiv:1906.03731*, 2019.
- [53] M. Simon and E. Rodner. Neural activation constellations: Unsupervised part model discovery with convolutional networks. In *Proceedings of the IEEE International Conference on Computer Vision*, pages 1143–1151, 2015.
- [54] G. Singh, Y. Kim, and S. Ahn. Neural systematic binder. In *The Eleventh International Conference on Learning Representations*, 2023.
- [55] D. Smilkov, N. Thorat, B. Kim, F. Viégas, and M. Wattenberg. Smoothgrad: removing noise by adding noise. *arXiv preprint arXiv:1706.03825*, 2017.
- [56] J. Su, D. V. Vargas, and K. Sakurai. One pixel attack for fooling deep neural networks. *IEEE Transactions on Evolutionary Computation*, 23(5):828–841, 2019.
- [57] M. Sundararajan, A. Taly, and Q. Yan. Axiomatic attribution for deep networks. In *International Conference on Machine Learning*, pages 3319–3328. PMLR, 2017.
- [58] A. Van Den Oord, N. Kalchbrenner, and K. Kavukcuoglu. Pixel recurrent neural networks. In *International Conference on Machine Learning*, pages 1747–1756. PMLR, 2016.
- [59] A. Vaswani, N. Shazeer, N. Parmar, J. Uszkoreit, L. Jones, A. N. Gomez, Ł. Kaiser, and I. Polosukhin. Attention is all you need. *Advances in Neural Information Processing Systems*, 30, 2017.
- [60] O. Vinyals, S. Bengio, and M. Kudlur. Order matters: Sequence to sequence for sets. *arXiv preprint arXiv:1511.06391*, 2015.
- [61] C. Wah, S. Branson, P. Welinder, P. Perona, and S. Belongie. Caltech–UCSD Birds-200-2011 (CUB-200-2011) dataset. Technical Report CNS-TR-2011-001, California Institute of Technology, 2011.
- [62] D. Wang, Z. Shen, J. Shao, W. Zhang, X. Xue, and Z. Zhang. Multiple granularity descriptors for fine-grained categorization. In *Proceedings of the IEEE International Conference on Computer Vision*, pages 2399–2406, 2015.
- [63] S. Wiegreffe and Y. Pinter. Attention is not not explanation. *arXiv preprint arXiv:1908.04626*, 2019.
- [64] Z. Wu, N. Dvornik, K. Greff, T. Kipf, and A. Garg. Slotformer: Unsupervised visual dynamics simulation with object-centric models. *arXiv preprint arXiv:2210.05861*, 2022.
- [65] T. Xiao, Y. Xu, K. Yang, J. Zhang, Y. Peng, and Z. Zhang. The application of two-level attention models in deep convolutional neural network for fine-grained image classification. In *Proceedings of the IEEE Conference on Computer Vision and Pattern Recognition*, pages 842–850, 2015.
- [66] M. Xue, Q. Huang, H. Zhang, L. Cheng, J. Song, M. Wu, and M. Song. ProtoPFormer: Concentrating on prototypical parts in vision transformers for interpretable image recognition. *arXiv preprint arXiv:2208.10431*, 2022.
- [67] C.-K. Yeh, B. Kim, S. Arik, C.-L. Li, T. Pfister, and P. Ravikumar. On completeness-aware concept-based explanations in deep neural networks. *Advances in Neural Information Processing Systems*, 33:20554–20565, 2020.
- [68] J. Yosinski, J. Clune, A. Nguyen, T. Fuchs, and H. Lipson. Understanding neural networks through deep visualization. *arXiv preprint arXiv:1506.06579*, 2015.
- [69] S. Zagoruyko and N. Komodakis. Wide residual networks. *arXiv preprint arXiv:1605.07146*, 2016.

- [70] M. Zaheer, S. Kottur, S. Ravanbakhsh, B. Poczos, R. R. Salakhutdinov, and A. J. Smola. Deep sets. *Advances in Neural Information Processing Systems*, 30, 2017.
- [71] M. E. Zarlenga, P. Barbiero, G. Ciravegna, G. Marra, F. Giannini, M. Diligenti, F. Precioso, S. Melacci, A. Weller, P. Lio, et al. Concept embedding models. In *NeurIPS 2022-36th Conference on Neural Information Processing Systems*, 2022.
- [72] H. Zhang, T. Xu, M. Elhoseiny, X. Huang, S. Zhang, A. Elgammal, and D. Metaxas. Spda-cnn: Unifying semantic part detection and abstraction for fine-grained recognition. In *Proceedings of the IEEE Conference on Computer Vision and Pattern Recognition*, pages 1143–1152, 2016.
- [73] N. Zhang, J. Donahue, R. Girshick, and T. Darrell. Part-based R-CNNs for fine-grained category detection. In *Computer Vision–ECCV 2014: 13th European Conference, Zurich, Switzerland, September 6–12, 2014, Proceedings, Part I 13*, pages 834–849. Springer, 2014.
- [74] H. Zheng, J. Fu, T. Mei, and J. Luo. Learning multi-attention convolutional neural network for fine-grained image recognition. In *Proceedings of the IEEE International Conference on Computer Vision*, pages 5209–5217, 2017.
- [75] B. Zhou, A. Khosla, A. Lapedriza, A. Oliva, and A. Torralba. Learning deep features for discriminative localization. In *Proceedings of the IEEE Conference on Computer Vision and Pattern Recognition*, pages 2921–2929, 2016.
- [76] B. Zhou, Y. Sun, D. Bau, and A. Torralba. Interpretable basis decomposition for visual explanation. In *Proceedings of the European Conference on Computer Vision (ECCV)*, pages 119–134, 2018.

Supplementary Material

A Reproducibility

All source codes, figures, models and etc., are available at https://github.com/jyhong0304/concept_centric_transformers.

B Method Details

Algorithm. Algorithm 1 shows the details of the Concept-Slot-Attention (CSA) module in our Cocent-Centric Transformer (CCT) in pseudo-code.

Comparison with Concept Transformers [49]. The concept embedding representation in our CCT is more sophisticated and generalizable than the one in Concept Transformers (CTs). Each concept embedding in CT is represented as a simple learnable vector shared with all input batches to learn. As such, it may be difficult for the vector to capture which image features can contribute to each concept more than others. For instance, as shown in Fig. 1 in the main text, given three images belonging to the same class “Winter Wren”, the image features with the same spatial positions from each image can have different importance for providing information to learn the same global concept, such as “*what is the main body color for Winter Wren?*” or “*what is the body shape for it?*”. In contrast, our proposed module naturally aggregates how much each image feature contributes to each concept using the attention \mathbf{A}^{CSA} (See in Algorithm 1) and provides batch-specific concept embedding representations that have more semantically meaningful information.

C Further Experimental Results and Details

In this section, we explain further experimental results and details. All experiments are conducted with three different random seeds and 95% confidence intervals.

C.1 Dataset Statistics

Table A-1 depicts the statistics of all benchmark datasets in our experiments. Because all datasets have no portion of validation, we manually pick the portion of the validation dataset for exploring the best hyperparameters for models.

For CUB-200-2011, we explain the pre-processing steps following [49]. Initially, the dataset has 312 binary attributes, but we filter to retain only those attributes that occur in at least 45% of all samples in a given class and occur in at least 8 classes. Thus, we get a total of 108 attributes, and based on this, we group them into two kinds of concepts: spatial and global con-

Algorithm 1 Concept-Slot-Attention (CSA) module. The module receives the set of input features $\mathbf{E} \in \mathbb{R}^{L \times D}$; the number of concepts C ; and the dimension of concepts d . The model parameters include: the linear projection $q^{\text{CSA}}, k^{\text{CSA}}, v^{\text{CSA}}$ with output dimension d ; a GRU network; a Gaussian distribution’s mean and diagonal covariance $\mu, \sigma \in \mathbb{R}^d$. In our experiments, we set the number of iterations to $T = 1$.

```
 $\mathbf{S}^{\text{concept}} = \text{Tensor}(C, d)$   $\triangleright \text{concept} - \text{slots} \in \mathbb{R}^{C \times d}$ 
 $\mathbf{S}^{\text{concept}} \sim \mathcal{N}(\mu, \sigma)$ 
 $\mathbf{E} = \text{LayerNorm}(\mathbf{E})$ 
for  $t = 0, \dots, T$  do
   $\mathbf{S}^{\text{concept}} = \text{LayerNorm}(\mathbf{S}^{\text{concept}})$ 
   $\mathbf{A}^{\text{CSA}} = \text{softmax}(\frac{1}{\sqrt{d}} q^{\text{CSA}}(\mathbf{S}^{\text{concept}}) \cdot k^{\text{CSA}}(\mathbf{E})^\top, \text{axis} = ' \text{concept} - \text{slots}' )$ 
   $\mathbf{A}^{\text{CSA}} = \mathbf{A}^{\text{CSA}} / \mathbf{A}^{\text{CSA}}.\text{sum}(\text{axis} = ' \text{inputs}', \text{keepdim} = \text{True})$ 
   $\mathbf{U} = \mathbf{A}^{\text{CSA}} \cdot v^{\text{CSA}}(\mathbf{E})$ 
   $\mathbf{S}^{\text{concept}} = \text{GRU}(\text{state} = \mathbf{S}^{\text{concept}}, \text{inputs} = \mathbf{U})$ 
end for
return  $\mathbf{S}^{\text{concept}}$ 
```

cepts. By looking at each attribute, we finally get 13 global and 95 spatial concepts. For example, `has_shape::perching-like` and `has_primary_color::black` are global concepts, and `has_eye_color::black` and `has_forehead_color::yellow` are spatial concepts.

C.2 Hardware Specification of The Server

The hardware specification of the server that we used to experiment is as follows:

- CPU: Intel® Core™ i7-6950X CPU @ 3.00GHz (up to 3.50 GHz)
- RAM: 128 GB (DDR4 2400MHz)
- GPU: NVIDIA GeForce Titan Xp GP102 (Pascal architecture, 3840 CUDA Cores @ 1.6 GHz, 384-bit bus width, 12 GB GDDR 5X memory)

C.3 Model Architectures

Variants of ViT. In our experiments, we use two variants of Vision Transformer (ViT), ViT-Large and ViT-Tiny, and employ timm Python library supported by Hugging Face™ (`vit_tiny_patch16_224` and `vit_large_patch16_224`). These variants are defined by their number of encoder blocks, the number of attention heads on each block, and the dimension of the hidden layer. The ViT-Large has 24 encoder blocks with 16 heads, and the dimension of the hidden layer is 1024. On the other hand, the ViT-Tiny has 12 encoder blocks with 3 heads, and the dimension of the hidden layer is 192, which is much more lightweight. A comparison between the variants of the ViT is shown in Table A-2.

C.4 MNIST Odd/Even Experiments

Additional Results. We describe the additional experimental results of CT and our CCT modules with full training samples and 10 epochs. In that setting, CT and CCT achieve $97.9_{\pm 0.4}\%$ and $98.9_{\pm 0.3}\%$ test accuracies, respectively ($\text{AVG}_{\pm \text{SD}}\%$). We see a marginal gap between the above performances, but Fig. A-1 shows that our CCT converges much faster than CT.

Hyperparameter Settings. We refer to the official implementation of CT [49] and do the experiments to produce Fig. 2 and Fig. 3 in the main text. For the experiments with different numbers of training samples (Fig. 2), we set the number of epochs to 150 and choose the number of training samples from the range from 100 to 3000 for both CT and CCT. For the experiments with full training samples and a small number of epochs (Fig. 3), we set the number of epochs to 10 for both methods. The only difference in hyperparameter settings between our CCT and CT is the learning rate for the AdamW [44] optimizer, $4e-4$ for CT, and $1e-3$ for our CCT. Table A-3a shows the shared hyperparameters for both approaches.

C.5 CIFAR100 Super-class Experiments

The Difference Between CCT and Other Deep-Learning Approaches with Logical Constraints. The logical constraint by [14] to address this task was introduced, i.e., once the model classifies an image into a class, the predicted probabilities of that super-class must first arrive at the whole mass.

Table A-1: Benchmark Dataset Statistics. † indicates the rescaled size of inputs for the ViT backbone, which is different from the original sizes of the datasets.

Dataset	MNIST Odd/Even	CIFAR100 Super-class	CUB-200-2011
Input size	$1 \times 28 \times 28$	$3 \times 224 \times 224^\dagger$	$3 \times 224 \times 224^\dagger$
# Classes	2 (odd or even)	20 (super-class)	200 (bird species)
# Concepts	10 (digit)	100 (class)	13 (global), 95 (spatial)
# Training samples	55,000	55,000	5,994
# Validation samples	5,000	5,000	1,000
# Test samples	10,000	10,000	4,794

Model	Layers	Hidden Dim.	Heads	# Params.
ViT-Tiny	12	192	3	5M
ViT-Large [12]	24	1024	16	304 M

Table A-2: Comparison between variants of the ViT

Referring to this, several deep-learning approaches leverage it [24, 39]. For instance, the five classes, *baby*, *boy*, *girl*, *man*, and *woman*, belong to the super-class *people*. Thus, $\Pr_{people}(\mathbf{x}) = 1$ if \mathbf{x} is classified as *baby*. So, logical constraints can be formulated as $\bigwedge_{s \in superclass} (\Pr_s(\mathbf{x}) = 0 \vee \Pr_s(\mathbf{x}) = 1)$, where the probability of the super-class is the sum of its corresponding classes' probabilities, e.g., $\Pr_{people}(\mathbf{x}) = \Pr_{baby}(\mathbf{x}) + \Pr_{boy}(\mathbf{x}) + \Pr_{girl}(\mathbf{x}) + \Pr_{man}(\mathbf{x}) + \Pr_{woman}(\mathbf{x})$.

However, because our CCT (and CT) follows Proposition 1 in [49], the probability of choosing the preferred superclass is $s^c = \arg \max_s (\beta_c)_s$ of class c (Refer to Eq.(1) in the main text). This means the super-class is determined by the largest attention score of the class among all classes, which is different from the definition of the logical constraint above.

Additional Results. Fig. A-2 showcases several examples of correct predictions by CT and our CCT, highlighting that compared to CT, our CCT achieves sparser explanation attention scores, which indicates a more confident and robust degree of belief for decision-making.

Fig. A-3 depicts the comparison of validation accuracy and explanation loss among ViT-Tiny, CT, and CCT. Compared to CT, CCT shows two stages of the learning process. In the first stage, CCT learns much faster than CT and quickly reaches a certain level of accuracy. Then, in the second learning stage, CCT fine-tunes itself by drastically reducing the explanation loss, and its accuracy is improved a bit more.

Hyperparameter Settings. For the experimental results, including Table 1 and Fig. 4 in the main text, referring to [14], we first find the best experimental setups of both ViT-Tiny and CT because they have not been evaluated on CIFAR100 Super-class before. Once the hyperparameter setup for the ViT-Tiny backbone is found to achieve similar performance to the Wide ResNet (the backbone for the second baseline group), we apply the same hyperparameter setting to both CT and our CCT. Table A-3b presents all shared hyperparameters for ViT-Tiny, CT, and our CCT.

C.6 CUB-200-2011 Experiments

Additional Results. We introduce additional experimental results to compare predictions between CT and our CCT. Fig. A-4 demonstrate the examples where our CCT outperforms CT to classify *Olive_sided_Flycatcher*. All CT's predictions were *Western_Wood_Pewee*, and this is caused by their spatial explanations, including `has_eye_color::black` and `has_leg_color::black`.

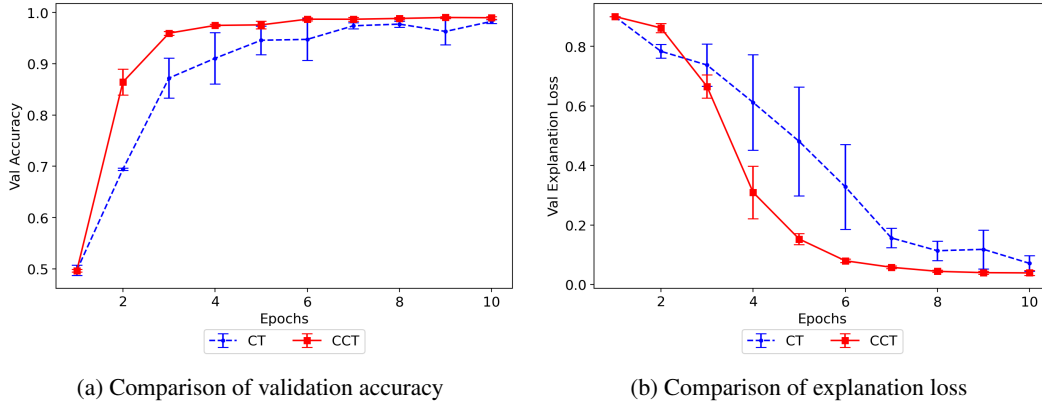


Figure A-1: Comparison between CT and CCT trained with full training dataset and 10 epochs on the MNIST Odd/Even dataset.

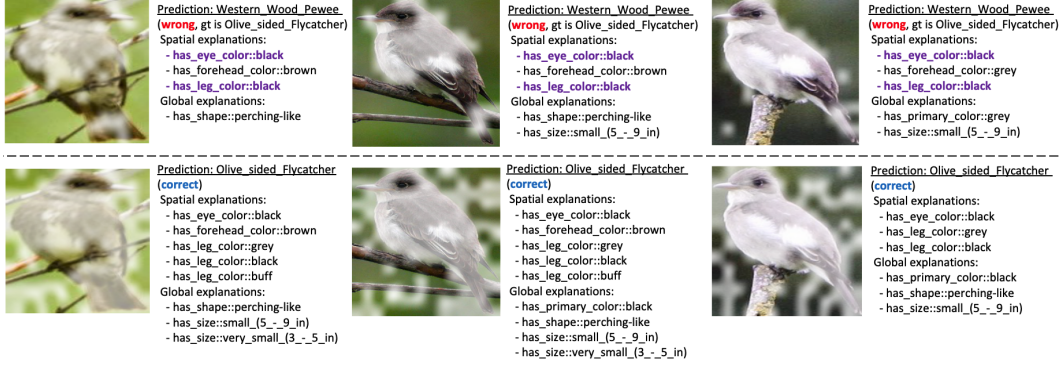


Figure A-4: Prediction comparison between CT and CCT. **(Top Row)** CT's predictions are incorrect. The purple highlighted explanations are key attributes in Western_Wood_Pewee. **(Bottom Row)** All predictions are correct by our CCT.

Name	Value	Name	Value	Name	Value
Batch size	32	Batch size	64	Batch size	16
Warmup Iters.	20	Epochs	20	Epochs	50
Explanation loss λ	2.0	Warmup Iters.	10	Warmup Iters.	10
Weight decay	1e-3	Learning rate	5e-5	Explanation loss λ	1.0
		Explanation loss λ	1.0	Weight decay	1e-3
		Weight decay	1e-3	Attention sparsity	0.5
		Attention sparsity	0.5		

(a) For both CT and CCT on MNIST Odd/Even

(b) For ViT-Tiny, CT and CCT on CIFAR100 Super-class

(c) For both CT and CCT on CUB-200-2011

Table A-3: Shared hyperparameters on different datasets.

Fig. A-5 demonstrates the comparison of validation accuracy and explanation loss between CT and CCT.

Hyperparameter Settings. We follow the official implementation of CT and produce the experimental results, including Table 2, Fig. 5, and Fig. 6 in the main text. The only difference in hyperparameter settings between our CCT and CT is the learning rate for the AdamW optimizer, 5e-5 for CT, and 1e-5 for our CCT. Table A-3c shows the shared hyperparameters for both approaches.

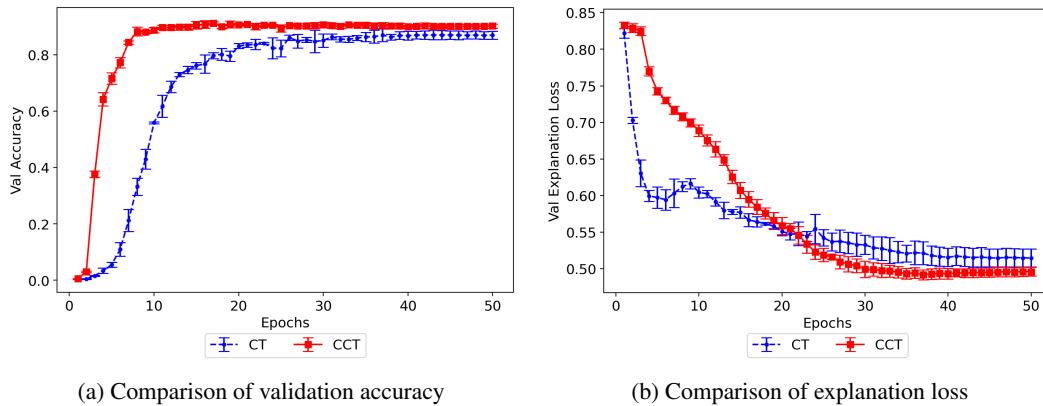


Figure A-5: Comparison between CT and CCT on the CUB-200-2011.

D Limitations

In this section, we explain the limitations of our proposed approach.

First, because of the CCT’s architectural characteristics in Section 3 in the main text, the proposed approach enforces additive contributions from the user-customized concepts to the classification probabilities. In other words, we ignore the latent higher-order relations among the concepts. For instance, in our CUB-200-2011 experiments, we assumed that global and spatial concepts could be represented and learned parallelly in our framework and that there is no correlation between the global concept and the spatial concept, which are independent. However, this is limited because more complex relationships, such as hierarchical properties, can exist among them. It might be addressed by introducing refined architectural properties in our CCT. For example, the Bi-directional Recurrent Unit can be introduced to allow global and spatial concepts to learn each other’s conceptual influences.

Secondly, although the domain expert’s knowledge is the most effective tool for guiding a model’s explainability, the pre-processing step to define the visual concepts for tasks may require time-consuming labeling and rely on human judgment. We also acknowledge that it needs to be overcome in our future research, and unsupervised concept extraction methods must be incorporated so that the model should provide explanations in semi-supervised or unsupervised fashions.